Journal of Materials Physics and Chemistry, 2013, Vol. 1, No. 4, 58-64
Available online at http://pubs.sciepub.com/jmpc/1/4/1

DOI:10.12691/jmpc-1-4-1

Time-evolution of Heat Affected Zone (HAZ) of Friction Stir Welds of AA7075-T651

A. Pastor[1], H. G. Svoboda[2,*]

[1]Sabato Institute, UNSAM/CNEA, San Martín, Argentina
[2]Materials and Structures Laboratory, INTECIN, Faculty of Engineering, University of Buenos Aires, Buenos Aires, Argentina
*Corresponding author: hsvobod@fi.uba.ar

Received October 08, 2013; Revised November 01, 2013; Accepted November 06, 2013

Abstract Friction Stir Welding (FSW) is a novel solid-phase welding process, which has proved to have a great potential for the realization of welded joints in materials with poor weldability such as heat-treatable aluminum alloys. However, the thermal cycles generated during FSW change the mechanical properties in heat affected zone (HAZ) due to two effects: over-age and re-dissolution of hardening precipitates. In other hand, the re-dissolved precipitates produce a evolution of both the microstructure and mechanical properties due to the natural aging phenomenon. The aim of this paper was to analyze the microstructural evolution in the HAZ of FSW joints in AA7075-T651 alloy. For this purpose samples FSW welded butt plate 4 mm in thickness. On the welded joint microstructural characterization was performed by light microscopy (LM), X-ray diffraction (XRD) and differential scanning calorimetry (DSC) and Vickers microhardness profiles (HV) after different elapsed times post welding. It was observed that the hardness increases with time after welding, due to the evolution of the phases present.

Keywords: *friction stir welding (FSW), AA7075-T651, heat affected zone (HAZ), differential scanning calorimetry (DSC)*

Cite This Article: A. Pastor, and H. G. Svoboda, "Time-evolution of Heat Affected Zone (HAZ) of Friction Stir Welds of AA7075-T651." *Journal of Materials Physics and Chemistry* 1, no. 4 (2013): 58-64. doi: 10.12691/jmpc-1-4-1.

1. Introduction

In recent decades, the industrial growth has driven the study of materials to meet the demanding requirements of new technologies. Undoubtedly, the aluminum has been one of the most studied materials for these purposes due to its good balance between mechanical properties and low density [1], which is essential in different industries such as aviation, aerospace, marine, automotive and rail [2,3]. One of the most important advances achieved, in the study of aluminum alloys, was the development of heat treatable aluminum alloys (HTAA). HTAA improve their mechanical strength by means of controlled precipitation of second phases [1,2,3,4] without a change in the density thereof. However, a great disadvantage of the most HTAA is their poor weldability by techniques involving melting.

In this context, the friction stir welding (FSW) shown a great potential for making joints in aluminum alloys considered not weldable [5,6,7]. The main characteristic of FSW is that avoid the problems associated with a solidification structure due to the fact that it is a solid phase welding. However, the thermal cycles generated during FSW welding affects the microstructure of heat treatable aluminum alloy. Hardening precipitates can suffer three phenomenons during the thermal cycles: dissolution, growth and coalescence [8,9,10]. These phenomenons cause a decrease in the mechanical strength of the material in different parts of the welded joint and create a minimum hardness zone (MHZ), which controls the mechanical properties of the weld. In turn, the re-dissolution of precipitates allows a potential re-precipitation due to the fact that many of these alloys exhibit natural aging [1], which generates a partial recovery of the mechanical properties in the joint [10,11] Although there are several studies regarding to FSW in HTAA, there is few information available on the study of the time-depending evolution of the microstructure and mechanical properties after welding. In this context, the objective of this paper is to study the temporal evolution of the microstructure of the HAZ of welded joints by FSW in AA7075 - T651 aluminum alloys and its influence on mechanical properties.

2. Experimental Procedure

The base metal used in this study was a 7075-T651 aluminum alloy plate of 4 mm in thickness, 150 mm in length and 75 mm in width. Two plates were clamped to avoid the separation during the welding, Figure 1. Friction stir welds were carried out using a tool with a smooth cylindrical pin and smooth concave shoulder. The joints were performed with a rotation and travel speed of 680 RPM a 51 mm/min respectively, while the tool angle (angle between the tool axis and base metal surface) was of 2º. This welding parameter produce sound welds.

During the welding, thermal cycles were obtained using three thermocouples at different distances from the centerline of welding: 7.5, 14.5 and 21.5 mm.

Transverse sections were prepared for metallographic observation, from the welding coupons. On this sections were determined Vickers microhardness profiles for different natural aging times after welding. In turn, the welded specimens were sampled for machining transverse tensile specimens, according to ASTM E8M-11, which were tested to determining the tensile strength after 168, 480, 960 and 1440 hours after the welding.

Tensile strength of the base metal was determined to calculate the joint efficiency of each welded joint at different aging times.

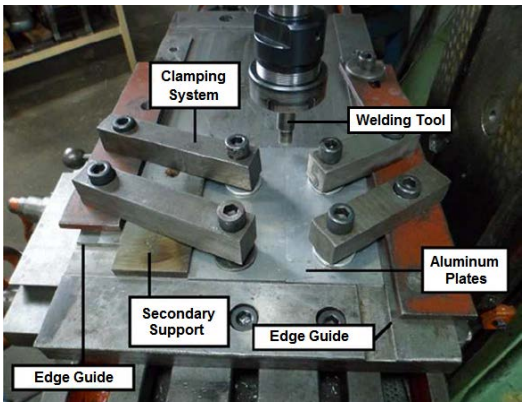

Figure 1. Experimental assembly for FSW

Samples were removed from the transverse section of the welding for analysis by Differential Scanning Calorimetry (DSC). These specimens were taken from the minimum hardness zone (MHZ) of the welded joint, which was determined in the microhardness profile. Once extracted the samples with a size of 2 mm^3 (1x1x2 mm) from the MHZ, they were washed with acetone in an ultrasonic washer and weighed on an analytical balance. Finally, the samples were encapsulated in high purity aluminum, previously to make the colorimetric assay. For DSC tests was used a Shimadzu DSC 60 equipment. All assays were performed with a heating rate of 10 °C/min within a temperature range from 100 °C to 350 °C. The base material and MHZ with 48, 720 and 1920 hours after welding were tested by DSC to analyze the influence of natural aging time on the structure of the precipitates.

3. Results and Discussions

3.1. Material

Table 1 shows the chemical composition of 7075-T651 aluminum alloy used in this work.

Table 1. Chemical composition of AA7075-T651

Material	Weight Percent (%wt)								
	Zn	Cu	Mg	Si	Fe	Mn	Cr	Ti	Al
AA 7075-T651	6.2	1.7	2.7	0.1	0.2	0.1	0.2	0.02	Bal.

7075 aluminum alloy incorporate Zn, Mg and Cu as principal alloy elements, which form the hardener precipitates during the heat treatment of aging this alloy. Figure 2a and Figure 2b show the microstructure of the base material, corresponding to the transverse and longitudinal section respect to rolling direction respectively. Figure 2c shows the spectrum of X-ray diffraction of the aluminum alloy.

The T651 designation for this alloy involves that the aging treatment was conducted at 120 °C for 24 hours, thus reaching to the peak hardening (maximum hardening available) of this alloy. Furthermore, because of the forming steps to which aluminum plates are subjected, elongated grains are observed in the rolling direction. The average hardness (HV1kg) of the material, measured on a transverse section was 183HV.

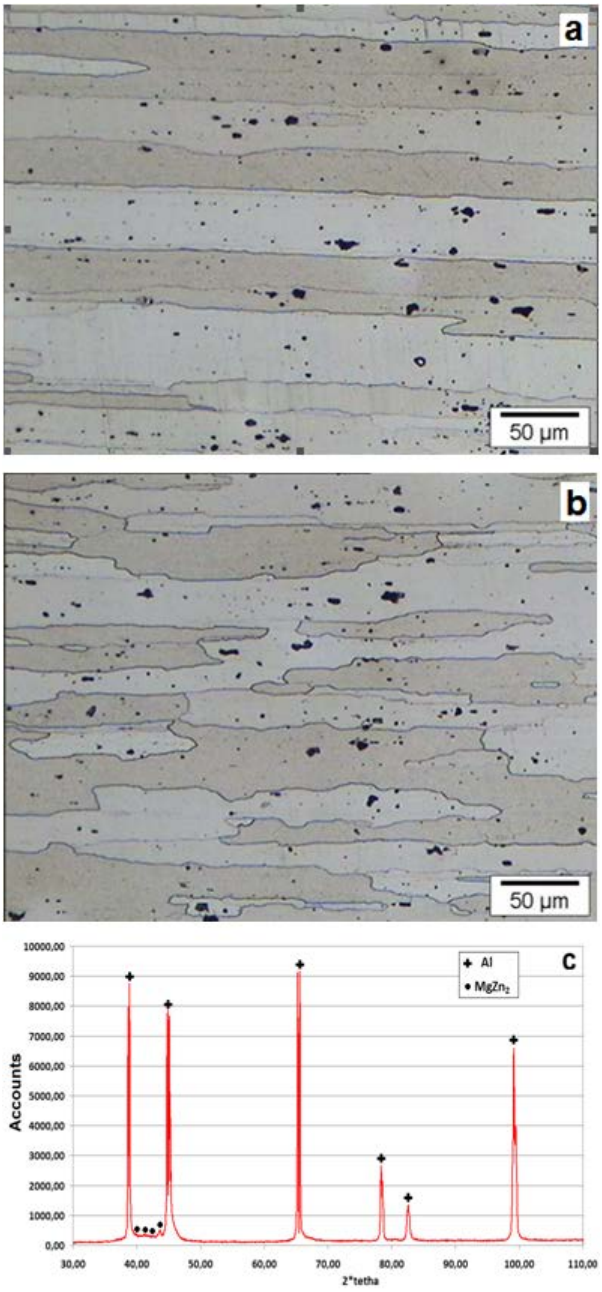

Figure 2. AA7075-T651: a) microstructure on a longitudinal section, b) microstructure on a cross section and c) X-ray diffraction (XRD) pattern

In the XRD spectrum (Figure 2c), the peaks indicated with a cross correspond to the solid solution of aluminum, while the peaks indicated by a circle corresponding to the phase $MgZn_2$. This composition corresponds to the η' and η phase formed during the artificial aging treatment of this alloy. It is important to note that η' is the phase that best

combines mechanical strength with stability [11] in this alloy. η phase is the majority phase in the over ageing stage and this tends to reduce the strength of the alloy due to the low capacity of opposition to the movement of dislocations, compared with the phases η '[4].

The sequence of precipitation of the hardening phases in the 7075-T6 aluminum is as follows [11]: Solid solution (SS) ➔ GPZ ➔ η' ($MgZn_2$) ➔ η ($MgZn_2$). Guinier-Preston zone (GPZ) are produced by the decomposition of the supersaturated solid solution and formed in a temperature range of 20 to 125 °C, at equilibrium conditions. These phases have low stability and quickly evolve into more stable structures formed at higher temperatures, such as η' and η phases. At temperatures between 130 and 290 °C, the metastable η' phase ($MgZn_2$) is formed. This metastable phase have a semicoherent interface with the matrix, so is more stable than GPZ, which forms a incoherent interphase with the matrix. It is important to note that there are phases precursor for the formation of η', known as η_1'. These phases have the same structure of η ', but they have a smaller size and their stability is comparable to GPZ. At temperatures above 290 °C, the stable η phase ($MgZn_2$) is formed. Both η' and η have hexagonal structure, but the lattice parameters is different [11]. It is important to note that the phases of greater stability, particularly η phases ($MgZn_2$) in the 7075 alloy, have low capacity to harden due to its high coherence with the matrix. In the other hand, the GPZ have a great capacity to harden due to its high incoherence with the matrix, however its stability is too slow. η' ($MgZn_2$) phases have greater ability to harden this alloy due to the fact that combine stability and incoherence with the matrix.

3.2. Welding

Figure 3a and Figure 3b shown a image of the welding coupon with the condition described above and the thermal cycles obtained to different distances from the center line of the welding respectively.

In order to analyze the thermal effect on the HAZ of the weld, particularly the MHZ, it is necessary to analyze the thermal cycles. Figure 3b thermal cycles are observed during welding at different distances from the center of the binding [12]. Since the shoulder of the tool used had a diameter of 12 mm, the thermal cycle obtained at 7.5 mm from the center of the joint is located at 1.5 mm from the edge of the joint, corresponding to the location of the area the ZMD, according to the hardness profiles (see Figure 6).

The dashed line in Figure 3b indicates the solvus temperature that separates α - β region (aging/overaging region) of α region (region of dissolution of precipitates) for composition of the alloy used in this work [1]. In the temperatures above of the dashed line the aluminum 7075-T651 remains in the region of dissolution of precipitates, while below of the dashed line the material is within the aging region. According to the thermal cycle taken at 7.5 mm, corresponding to the MHZ can be seen that this zone remains in the region corresponding to temperatures of dissolution of precipitates for over 50 seconds. As reported in the literature [11,13,14], this time is long enough to cause redisolution of some fraction of the hardening phases, primarily the phases with low stability (ZGP and η_1'). Additionally, the heat cycle generated during welding can produce the overaging of the most stable phase [8,9,10], which are not dissolved to these temperatures. Both redisolution of low-stability hardening phases as the overaging of the stable hardening phases tend to reduce the hardness and strength of the material. However, the redisolution of the low-stability hardening phases leaves in solid solution a significant fraction of alloying elements, which have the potentiality to precipitate again by a aging heat treatment. In this aspect, AA7075 alloys show a particular behavior, because the aging phenomenon (controlled precipitation of the dissolved alloying elements) can occur at room temperature. This is known as natural aging.

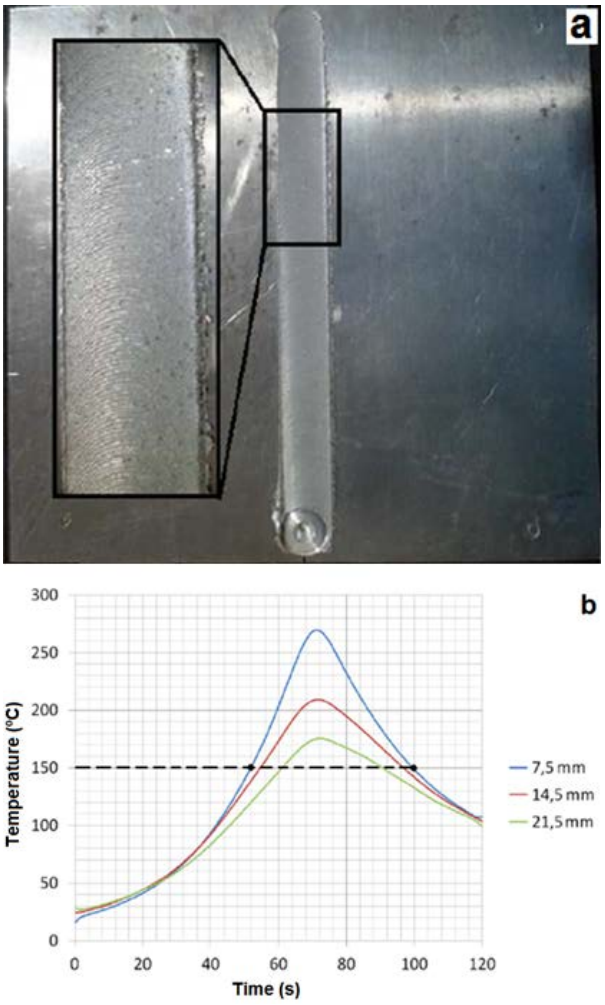

Figure 3. a) AA7075-T651 welded sample by FSW, b) Thermal cycles taken at different distances from the center line of the welding

3.3. Microstructural Characterization

Figure 4 shows the micrograph obtained from transverse section of the welding. In this micrograph are shown the characteristic zones of the welding joint by FSW. No macroscopic defects were observed in the welded joint.

Figure 4. Macrostructure of FSW welded joint: 1- Stir Zone, 2- Thermo-mechanically affected zone (TMAZ), 3- Heat affected zone (HAZ), and 4- Base metal (BM)

Figure 5 shows the micrographics of the different zones of the welded joints by FSW.

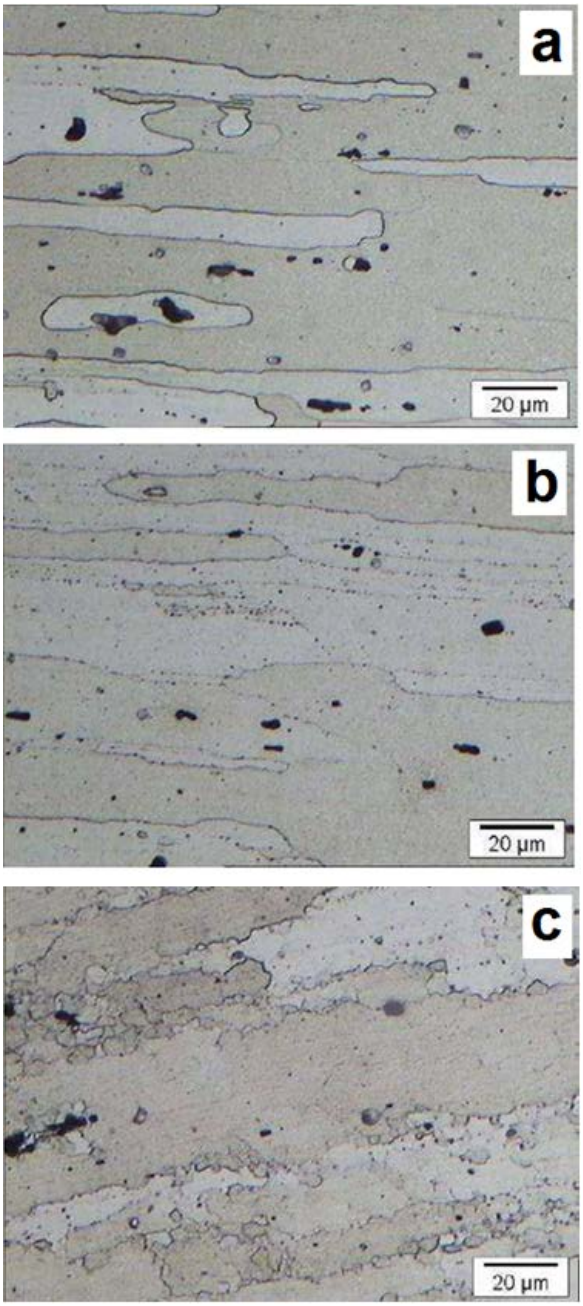

Figure 5. Microstructure of a) Heat affected zone (HAZ), b) Minimum hardness zone (MHZ), and c) Thermo-mechanically affected zone (TMAZ)

There are no difference between the microstructure of the TAZ (Figure 5a) and base metal (Figure 2b), however the MHZ (Figure 5b) presents fine precipitates distributed in the grain boundaries. TMAZ (Figure 5c). The TMAZ (Figure 5c) shows the presence of the plastic deformation, partial recrystallization and precipitation in the grains of the aluminum microstructure. It is important to note that, for the welding condition sampled, MHZ is included in the TAZ. However, other works shown that the MHZ can be displaced to the TMAZ by decreasing the heat input [16].

3.4. Microhardness

Figure 6 shows the Vickers hardness profile (HV1kg) determined on the transverse section of the welded joint at different times after completion of the welding.

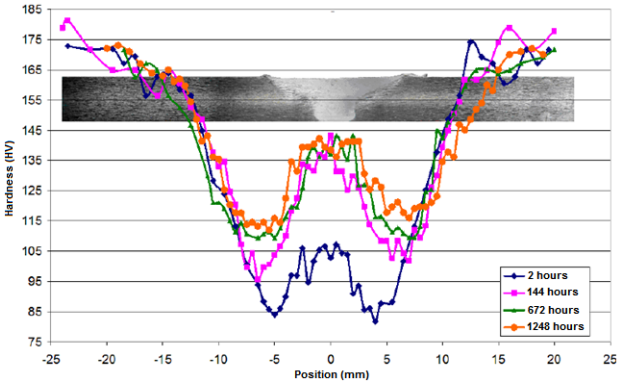

Figure 6. Microhardness Vickers profiles obtained at different times after the welding

Typical W-shaped hardness profiles of welded joints obtained by FSW in heat treatable aluminum alloys [5,6] were observed, showing the existence of the MHZ. In this hardness profiles can be observed that the MHZ is located to 7.5 mm from the center line of the joint, coinciding with thermal cycling to 7.5 mm (Figure 3b). The decrease in hardness in the MHZ is associated with the redisolution and overaging phenomena [8,9,10] above mentioned. Can be noted that this drop in the hardness is really significant, since a minimum value of 80 HV after 2 hours of the welding was observed, significantly lower than the base material 183 HV (0.43 HV_{MB}). On the other hand, Figure 6 shows the evolution of the hardness profiles, where a increases of the hardness were observed with time, reaching values of 120 HV to 1248 h (52 days) after the welding in the MHZ (0.66 HV_{MB}). It has been reported in the literature that the evolution of the hardness has a logarithmic evolution [17].

3.5. Differential Scanning Calorimetry

Figure 7 shows the thermograms of base metal and MHZ. The calorimetric curves of the MHZ were performed at different times after welding to analyze the influence of the natural aging.

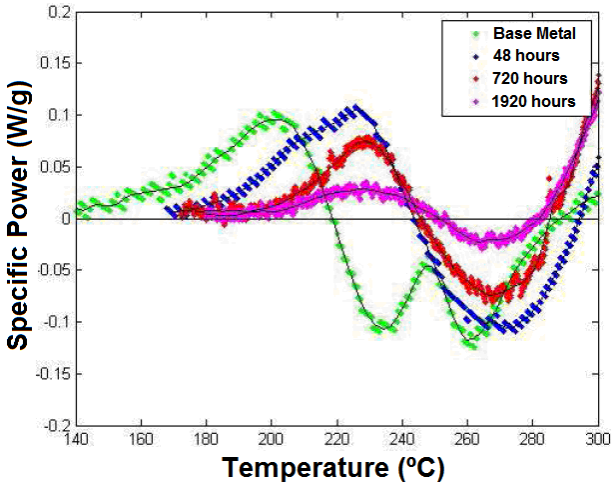

Figure 7. Calorimetric curves obtained from base metal and MHZ at different times (48, 720 and 1920 hours) after the welding

It can be observed several differences between the thermograms of the material removed from the MHZ, which was naturally aged for different times, respect to the thermogram presented by the base metal, which was

subjected to an artificial aging treatment to obtain the peak hardening of the alloy. Although there are kinetic differences between the reactions that occur in the natural aging as compared to artificially aging [11,15], it is accepted that the first endothermic peak corresponds to the dissolution of the low-stability hardening phases (ZGP and η_1), while the second exothermic peak involves three reactions: η' formation, η' dissolution and η formation. When comparing the results of naturally-aged alloys after welding with those of the base metal (artificially aged), it is can be identified two phenomenon: a) the endothermic reaction peak (first peak) of the base metal is shifted towards higher temperatures after welding and b) the double-exothermic peak in the base metal is replaced by a single exothermic peak, which tends to disappear with increasing natural aging time.

To explain this tendency in the thermograms at different times of natural aging is necessary to consider the reactions that involve each peak. As mentioned above, the first endothermic peak is associated with the dissolution of low-stability phases present in the material prior to welding. Although in the literature there is no agreement about what phases are dissolved in the first endothermic peak [10,11,15], in most cases it is accepted that this corresponds to the dissolution of GPZ and η_1' (η' precursor). Regarding to the temperature range where the exothermic reaction peak appears, it is important to note, as mentioned before, that occurs three reactions within this range: η' formation, η' dissolution and η formation. Notably, the latter reaction usually is overlapped with the dissolution reaction of the η' phase. The extent of each reaction determines the nature and form of the second peak.

With increasing natural aging time, thermograms show that the first peak (endothermic) tends to: a) decrease its area under the curve and b) displace the reaction peak to higher temperatures. The decrease in the area under the peak indicates a lower fraction of phases that are dissolved at this temperature. This behavior can be explained considering that the ZGP and η_1' phases are formed firstly after redissolution generated by the welding thermal cycles and quickly tend to evolve to more stable phase, in this case η'. Therefore, when the natural aging time is increased, the fraction of lower-stable phases (GPZ and η_1') is decreased, because they evolve to more stable phase by natural aging, so the area under the curve of first endothermic peak decrease. Regarding to displacement of first reaction peak to higher temperatures, it is necessary to consider that the increase of aging time promotes an increased stability of the present phases. Less stable phases increase their stability until eventually they become more stable phases. It is obvious that GPZ and η_1' phases, which are dissolved at higher aging time, are more stable, so they need more energy to be dissolved, therefore the reaction peak is displaced to higher temperatures.

Regarding to the analysis of the second reaction peak (exothermic), Figure 7 shows that the area of exothermic peak is decreased when the natural aging time increases. In order to achieve a better compression of the behavior of the exothermic peak observed in Figure 7, Figure 8 shows a scheme of the reactions involved in the second reaction peak during the calorimetric analysis at different aging times.

To analyze the trend observed in the second reaction peak it is important to consider the following factors: a) there is an equilibrium concentration of each phase under this conditions of temperature and heating rate, so during the calorimetric test it will precipitate only the phase fraction necessary to reach this concentration; b) low-stability phases tend to evolve to more stable phases during the natural aging; c) during the calorimetric test, the area under a peak of a precipitation reaction show the fraction that precipitate during the test only. However, the area under a peak of a dissolution reaction shows the dissolved fraction of a phase, regardless if it was formed during the test or prior the test.

The following precipitation reactions occur in 7075-T651 aluminum alloy during the natural aging: a) saturated solid solution to GPZ, and b) GPZ to η'. The η' to η reaction is not observed during the natural aging [11,15]. When natural aging time is increased, the η' fraction prior to the calorimetric test increases. Therefore the η' fraction able to precipitating to reach the equilibrium concentration during the calorimetric test is lower.

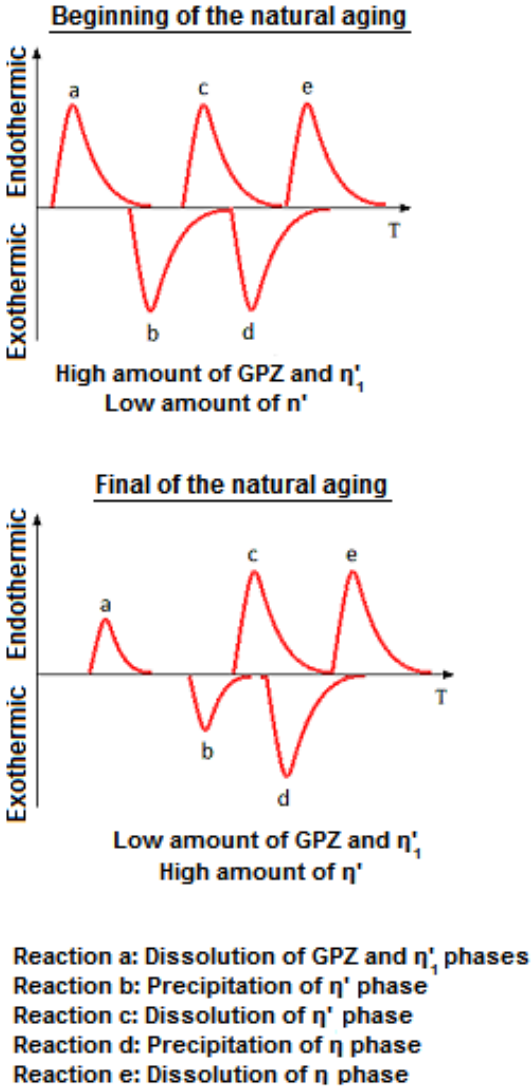

Figure 8. Schematic representation of the contributions involved in each reaction peak shown in the thermograms obtained at different aging times

So, the natural aging of the GPZ, which evolve to η' phase, is evidenced for the reduction of the area under the

precipitation peak of the η' phase. However, the area under the dissolution peak of η' phase (peak c) is not reduced when the natural aging time is increased, because it does not differentiate between the phases formed during (peak b) or prior to the calorimetric test. The sum of these two contributions (the area under the precipitation peak of η' phase (peak b) is reduced and the area under the dissolution peak of η' phase (peak c) is remained almost constant) at different natural aging times is the responsible of the reduction of the area under the exothermic peak in the Figure 7. These results agree with those reported in the literature, which shows that for high natural aging times the area under the exothermic peak is greatly reduced and, in some cases, has been reported that this peak becomes to a endothermic peak [11,15]. It is important to note the similarity that present the thermograms of the naturally aged samples taken from the MHZ (Figure 7), with the thermograms of RRA treatment (retrogression and artificial re-aging) of this alloy shown in Figure 9, reported in two different works [11,15].

This similarity is due to the fact that the thermal cycles of RRA treatment are very similar to those experienced by the 7075-T651 aluminum alloy during welding by FSW.

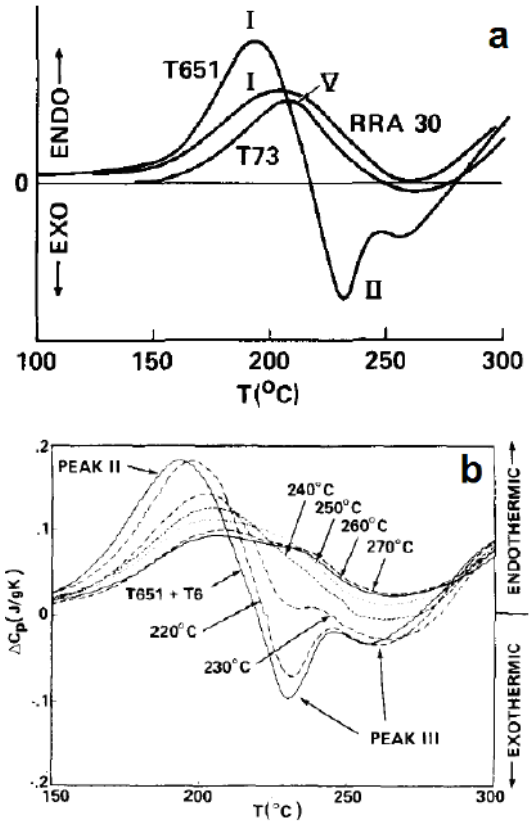

Figure 9. a) Thermograms of AA 7075 with different heat treatments (T651, T73 and RRA at 250ºC during 30s) [11], and b) Thermograms of AA 7075 with different heat treatments (T651 and RRA at indicated temperature during 30s) [15]

In the RRA treatment an artificially aged sample is solution annealed in the dissolution region of precipitates (region α) for a short time, and then it is re-aged. The result of this heat treatment is the reprecipitation and overaging, which achieves a good balance between the mechanical strength and corrosion resistance.

This is an interesting point of view, due to the large information and work done on heat treatments of this alloy and the lack of information related to the welding thermal cycle effect.

3.6. Tensile Properties

Table 2 shows the results of tensile testing of the analyzed conditions. The joint efficiency achieved is showed in each case.

Table 2. Tensile Strength of AA7075-T651 base metal and welded joints for different times after welding

Condition	Time (hours)	Tensile Strength (MPa)	Efficiency (%)
Base Metal	-	576	-
FSW-1	168	383	0.66
FSW-2	480	417	0.72
FSW-3	960	418	0.73
FSW-4	1440	421	0.73

Regarding to the influence of the natural aging on the tensile properties, an increase of the η' phase fraction on MHZ promotes an improvement of mechanical strength in this zone, as observed in the Table 2. This behavior is in accordance with the trend of the MHZ observed in Figure 6, where the increase of the natural aging time produces an increase of the microhardness in the MHZ. Figure 10 plots the evolution of the tensile strength and microhardness in MHZ with natural aging time.

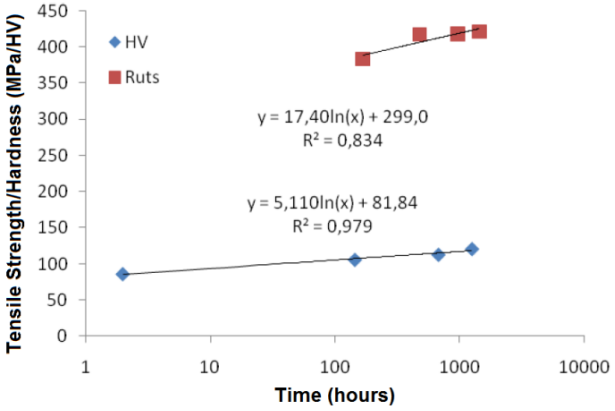

Figure 10. Variation of tensile strength and hardness of the welded joints at different natural aging times

It is important to note that the fractures in the tensile specimens were located in the MHZ, so that the correlation between the hardness and tensile strength in this zone is valid.

Both tensile strength and microhardness were adjusted using a logarithmic expression, according to that reported in the literature [5]. As can be seen, a good correlation was obtained for both the hardness and the tensile strength. Another important result to discuss is that, despite the partial recovery of mechanical properties, is no possible recover the mechanical properties of the base metal. This is observed in both the microhardness testing as well in the tensile tests. This is due to two factors: a) the natural aging does not achieve complete precipitation of all alloying elements that were introduced into solid solution because higher temperatures are required and b) welding thermal cycle overages a fraction of precipitates, so cannot be achieved the original mechanical properties because they are obtained in the peak hardening of the alloy, where over-aging does not occurs. Regarding to this last factor

has been reported [13] that the growth of the precipitates by overaging occurs first at the grain boundaries of the alloy. This result agrees with the micrographic analysis which shows an increase in the density of precipitates in the grain boundaries of the MHZ (Figure 5b), compared with the base metal. Therefore, the joint efficiency increases with the natural aging time, from 66% to 73% for 1440 hours (60 days) after welding by FSW. This is an important technological aspect since the joint efficiency is the considered for the design of welded structures.

4. Conclusions

Thermal cycles generated during FSW welding produce the redissolution of low-stability phases, such as GPZ and η_1', and the overaging of the phases more stable, such as η. This phenomenon promotes a severe softening (0, $45HV_{MB}$) and loss of mechanical properties in the HAZ. After welding the material affected for the thermal cycle evolutes with time due to a natural aging. It has been observed that the re-dissolved precipitates have the capacity to precipitate due to natural aging phenomenon, which promotes the formation of hardening phases as GPZ, η_1' and η'. These phases are responsible for the increase of the mechanical properties during of natural aging. Such recovery of the mechanical properties with the natural aging time evolves logarithmically with time, achieving at 1250 hours after the welding approximately 66% of the hardness and for 1440 hours 73% of the tensile strength of the base material. Furthermore, similarity was observed in the microstructural evolution between the naturally aged material and this alloy heat treated by RRA treatment.

Acknowledgements

The authors wants to acknowledge to the III International Congress of Science and Technology of Metallurgy and Materials, August 20-23 of 2013, Iguazú, Argentina), to Asociación Argentina de Materiales (SAM) and to University of Buenos Aires and ANPCYT for the financial support of this project.

Also expresses its grateful to Dr. Mariano Escobar for its collaboration with the DSC experiments.

References

[1] American Society for Metals (ASM). Properties and Selection: Nonferrous Alloys and Special-Purpose Materials (Vol. 2). 10 ma ed. Ohio: ASM International. 2005.

[2] J. Gilbert Kaufman "Introduction to Aluminum Alloys and Tempers", 2000, ASM International.

[3] J. R. Kissell and R. L. Ferry, "Aluminum Structures: A guide to their specifications and design", 2002, John Wiley and Sons, Inc.

[4] D.A. Porther, K.E. Easterling. "Phase transformation in metals and alloys", 1992, Chapman & Hall.

[5] R.S. Mishra and Z.Y. Ma, "Friction stir welding and processing". Materials Science and Engineering R, Vol. 50 (2005), p. 1-78.

[6] R. Nandan, T. DebRoy, H.K.D.H Bhadeshia. "Recent advances in friction-stir welding – Process, weldment structure and properties", Progress in Materials Science, Vol 53 (2008), p. 980-1023.

[7] W. Xu, J. Liu, G. Luan, C. Dong, "Microstructure and mechanical properties of friction stir welded joints in 2219-T6 aluminum alloy", Materials and Design, Vol. 30 (2009), p. 3460-3467.

[8] J.Q. Su, T.W. Nelson, R.S. Mishra, M.W. Mahoney. "Microstructural investigation of friction stir welded 7050-T651 aluminum", Acta Materialia, Vol 51 (2005), p. 713-718.

[9] K.V. Jata, K.K. Sankaran, J.J. Ruschau. "Friction stir welding effects on microstructure and fatigue of aluminum alloy 7050-T7451", Metallic Materials Transaction. A. Vol. 31 (2000), p. 2181-2187.

[10] C. B. Fuller, M. W. Mahoney, M. Calabrese, L. Micona. "Evolution of microstructure and mechanical properties in naturally aged 7050 and 7075 Al friction stir welds", Materials Science and Engineering A. Vol 527 (2010), p. 2233-2240.

[11] J.K. Park, A.J. Ardell. "Correlation between Microstructure and Calorimetric Behavior of Aluminum Alloy 7075 and AI-Zn-Mg Alloys in Various Tempers", Materials Science and Engineering A, Vol. 114 (1989), p. 197-203.

[12] L. N. Tufaro. "Tensiones Residuales y Propiedades Mecánicas de uniones Soldadas por Fricción-Agitación (FSW) de AA 7075-T651", Buenos Aires, Facultad de Ingeniería UBA, 2012.

[13] F. Viana, A.M.P. Pinto, H.M.C. Santos, A.B. Lopes. "Retrogression and re-ageing of 7075 aluminum alloy: microstructural characterization", Journal of Materials Processing Technology, Vol 92-93 (1999), p. 54-59

[14] A. Baldantoni. "On the microstructural changes during the retrogression and re-aging of 7075 type aluminum alloys". Materials Science Engineering. Vol 72: L5- L8. 527 (1985), p. 2233-2240.

[15] J.M. Papazian. "Differential Scanning Calorimetry Evaluation of Retrogressed and Re-aged Microstructures in Aluminum Alloy 7075". Materials Science Engineering 79 (1986), p. 97-104.

[16] A. E. Pastor. "Efecto de las variables del proceso de Soldadura por Fricción Agitación (FSW) de aleaciones de aluminio de alta resistencia sobre la microestructura y las propiedades mecánicas", Buenos Aires, Instituto de Tecnología Jorge Sabato, 2012.

[17] M. Ku, F. Hung, T. Lui and L. Chen, "Embrittlement Mechanism on Tensile Fracture of 7075 Al Alloy with Friction Stir Process (FSP)", Materials Transactions, Vol. 52, No. 1 (2011), pp. 112 to 117.